American Journal of Computational and Applied Mathematics 2012, 2(2): 33-41
DOI: 10.5923/j.ajcam.20120202.07

MHD-Conjugate Heat Transfer Analysis for Transient Free Convective Flow Past a Vertical Slender Hollow Cylinder

H. P. Rani*, G Janardhana Reddy

Department of Mathematics, National Institute of Technology, Warangal, 506004, India

Abstract In this paper the effects of magnetic field and conduction on the transient free convective boundary layer flow over a vertical slender hollow circular cylinder with the inner surface at a constant temperature are investigated. The transformed dimensionless governing equations for the flow and conjugate heat transfer are solved by using the implicit finite difference scheme. For the validation of the current numerical method heat transfer results for a Newtonian fluid case where the magnetic effect and conduction is zero are compared with those available in the existing literature, and an excellent agreement is obtained. Numerical results for the transient flow variables, average wall shear stress and average heat transfer rate are shown graphically. In all these profiles it is observed that the times needed to reach the steady-state and the temporal maximum increases as the magnetic parameter or conjugate heat transfer parameter increases.

Keywords Conjugate Heat Transfer, Magneto Hydrodynamic, Natural Convection, Vertical Slender Hollow Cylinder, Finite Difference Method

1. Introduction

Unsteady natural convection flows over vertical bodies have a wide range of applications in engineering and technology. In manufacturing processes such as hot extrusion, metal forming and crystal growing, heat transfer effects plays an important role. Free convection flow of air bathing a vertical cylinder with a prescribed surface temperature was first presented by Sparrow and Gregg[1] by applying the similarity method and power series expansion. Velusamy and Garg[2] presented the numerical solution for transient natural convection over heat generating vertical cylinders of various thermal capacities and radii. While Fujii and Uehara[3] analyzed the local heat transfer results for arbitrary Prandtl numbers. Lee et al.[4] investigated the similar problem along slender vertical cylinders and needles for the power-law variation in the wall temperature. In general, Ganesan and Rani[5] have investigated the unsteady natural convection flow over a vertical cylinder with variable heat and mass transfer using the finite difference method. Recently, Rani and Kim[6] investigated the unsteady effects for the similar problem with temperature dependent viscosity.

In these studies the wall conduction resistance for the convective heat transfer between a solid wall and a fluid flow was neglected considering a thin vertical wall. However, in practical systems the wall conduction resistances have a significant effect in the fluid flow and in the heat transfer characteristics in the vicinity of the wall. Thus the conduction in the solid wall and the convection in the fluid, known as conjugate heat transfer (CHT), should be determined simultaneously. These type of problems are usually referred to as conjugate heat transfer problems, and they have many practical applications, particularly those related to energy conservation in buildings, cold storage installations and cryogenic applications, such as medical and space technology. The CHT problems have been studied by several research groups[7-9] with the help of mathematical models for simple heat exchanger geometries. Gdalevich et al.[10] and Miyamoto et al.[11] reviewed the early theoretical and experimental works of the CHT problems for a viscous fluid. Miyamoto observed that a mixed-problem study of the natural convection has to be performed for an accurate analysis of the thermofluid-dynamic (TFD) field if the convective heat transfer depends strongly on the thermal boundary conditions. Pozzi et al.[12] investigated the entire TFD field resulting from the coupling of natural convection along and conduction inside a heated flat plate by means of two expansions, regular series and asymptotic expansions. Moreover, Vynnycky et al.[13] studied the two dimensional conjugate free convection for a vertical plate of finite extent adjacent to a semi-infinite porous medium using finite difference techniques. Recently, Kaya[14] studied the effects of buoyancy and CHT on non-Darcy mixed convection about a

* Corresponding author:
hprani@nitw.ac.in (H. P. Rani)
Published online at http://journal.sapub.org/ajcam

vertical slender hollow cylinder embedded in a porous medium with high porosity.

Also, magnetohydrodynamic (MHD) flow and heat transfer processes occur in many industrial applications such as the geothermal system, aerodynamic processes, chemical catalytic reactors and processes, spreading of chemical pollutants in plants. Moreover, effects of thermophoresis on hydromagnetic flow along a flat plate were studied by Chamkha and Camille [15]. Recently, Mamun et al.[16] investigated the effects of magnetic field, viscous dissipation and heat generation on natural convection flow along and conduction inside a vertical flat plate.

From the above studies, it can be noted that the CHT on the unsteady natural convective hydromagnetic flow of a viscous incompressible fluid over a vertical cylinder has received very scant attention in the literature. Hence, in the present investigation our attention is focused on the effect of magnetic field on the coupling of conduction inside and the laminar natural convection flow over the outside surface of a vertical slender hollow cylinder. The temperature of the inner surface of the cylinder is kept at a constant value which is higher than the ambient fluid temperature and the temperature of the outer surface is determined by the conjugate solution of the steady-state energy equation of the solid and the boundary layer equations of the fluid flow. The governing equations are solved numerically by the implicit finite difference method to obtain the transient velocity and temperature profiles, coefficient of skin-friction and heat transfer rate for different values of conjugate heat transfer and magnetic parameters.

In section 2, a detailed description about the formulation of the problem is given. Also, the governing equations, such as mass, momentum and energy equations of an incompressible fluid flow past a vertical cylinder are derived and non-dimensionalized. In section 3, the details about the grid generation and numerical methods for solving the above governing equations are given. In section 4, transient two-dimensional velocity and temperature profiles, average skin-friction coefficient and heat transfer rate are analyzed. Finally, the concluding remarks are made in section 5.

2. Formulation of the Problem

An unsteady two-dimensional laminar free convective hydromagnetic flow of a viscous incompressible fluid past a vertical slender hollow cylinder of length l and outer radius r_0 ($l >> r_0$) is considered as shown in Fig. 1. The x-axis is measured vertically upward along the axis of the cylinder. The origin of x is taken to be at the leading edge of the cylinder, where the boundary layer thickness is zero. The radial coordinate, r, is measured perpendicular to the axis of the cylinder. The surrounding stationary fluid temperature is assumed to be of ambient temperature (T'_∞). The temperature of the inside surface of the cylinder is maintained at a constant temperature of T'_0, where $T'_0 > T'_\infty$. Initially, i.e., at time $t' = 0$ it is assumed that the outer surface of the cylinder and the fluid are of the same temperature T'_∞. As time increases ($t' > 0$), the temperature of the outer surface of the cylinder is raised to the solid-fluid interface temperature T'_w and maintained at the same level for all time $t' > 0$. This temperature T'_w is determined by the conjugate solution of the steady-state energy equation of the solid and the boundary layer equations of the fluid flow and is discussed elsewhere. It is assumed that the effect of viscous dissipation is negligible in the energy equation. It is further assumed that the interaction of the induced axial magnetic field with the flow is considered to be negligible compared to the interaction of the applied magnetic field H_0, with the flow. Under these assumptions, the boundary layer equations of mass, momentum and energy with Boussinesq's approximation are as follows:

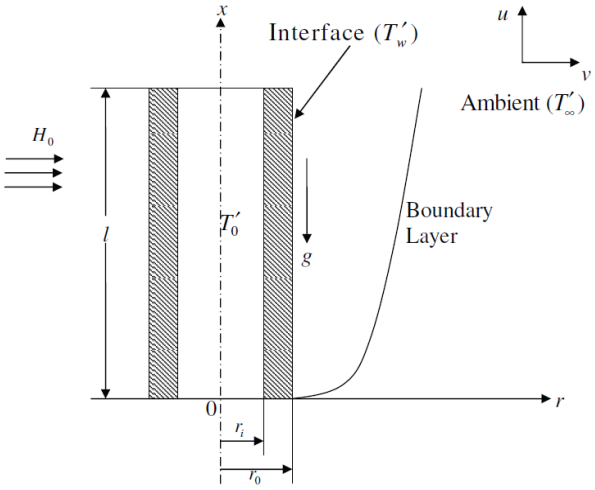

Figure 1. Schematic of the investigated problem

$$\frac{\partial (ru)}{\partial x} + \frac{\partial (rv)}{\partial r} = 0 \tag{1}$$

$$\rho\left(\frac{\partial u}{\partial t'} + u\frac{\partial u}{\partial x} + v\frac{\partial u}{\partial r}\right) =$$

$$\rho g\beta(T' - T'_\infty) + \frac{1}{r}\frac{\partial}{\partial r}\left(\mu r\frac{\partial u}{\partial r}\right) - \sigma H_0^2 u \tag{2}$$

$$\frac{\partial T'}{\partial t'} + u\frac{\partial T'}{\partial x} + v\frac{\partial T'}{\partial r} = \frac{\alpha}{r}\frac{\partial}{\partial r}\left(r\frac{\partial T'}{\partial r}\right) \tag{3}$$

The corresponding initial and boundary conditions are given by

$$\begin{aligned} &t' \le 0 \ : u = 0,\ v = 0,\ T' = T'_\infty \quad \text{for all } x \text{ and } r \\ &t' > 0 : \ u = 0,\ v = 0,\ T' = T'_w \quad \text{at} \quad r = r_0 \\ &\qquad u = 0,\ v = 0,\ T' = T'_\infty \quad \text{at} \quad x = 0 \\ &\qquad u \to 0,\ v \to 0,\ T' \to T'_\infty \quad \text{as} \quad r \to \infty \end{aligned} \tag{4}$$

where T'_w is the unknown solid-fluid interface temperature and is determined as follows:

To predict the outer surface temperature of the cylinder T'_w, an additional governing equation is required for the slender hollow cylinder based on the simplification that the wall of cylinder steady transfers its heat to the surrounding fluid. Since the outer radius of the hollow cylinder, r_0, is small compared to its length, l, the axial conduction term in

the heat conduction equation of the cylinder can be omitted. The governing equation for the temperature distribution within the slender hollow circular cylinder is given by Chang[17] as follows:

$$\frac{\partial^2 T_s'}{\partial r^2}+\frac{1}{r}\frac{\partial T_s'}{\partial r}=0;\quad 0\le x\le l;\ r_i\le r\le r_0 \tag{5}$$

subject to

$$\begin{aligned} T_s' &= T_0' \ \text{ at } \ r=r_i \\ T_s' &= T_w' = T'(x,r_0) \ \text{ at } \ r=r_0 \end{aligned} \tag{6}$$

The general solution of Eq. (5) along with (6) is given by

$$T_s' = T_0' + (T'(x,r_0)-T_0')\frac{\ln(r/r_i)}{\ln(r_0/r_i)} \tag{7}$$

On the other hand, Eq. (5) is coupled with the energy equation in the fluid region based on the condition that the temperature and the heat flux are continuous at the solid-fluid interface, namely

$$T_s' = T'(x,r_0),\ -k_s\frac{\partial T_s'}{\partial r} = -k_f\frac{\partial T'(x,r_0)}{\partial r} \ \text{ on } r=r_0 \tag{8}$$

Using Eqs. (7) and (8), the temperature distribution T_w' at the interface is given by

$$T_w' = T'(x,r_0) = r_0\frac{k_f}{k_s}\ln\left(\frac{r_0}{r_i}\right)\frac{\partial T'(x,r_0)}{\partial r}+T_0' \ \text{ at } r=r_0 \tag{9}$$

By introducing the following non-dimensional quantities

$$\begin{aligned} &X = Gr^{-1}\frac{x}{r_0},\ R=\frac{r}{r_0},\ U=Gr^{-1}\frac{u\,r_0}{\upsilon},\ V=\frac{v r_0}{\upsilon},\ t=\frac{\upsilon t'}{r_0^2}, \\ &T=\frac{T'-T_\infty'}{T_0'-T_\infty'}\ Gr=\frac{g\beta\, r_0^3(T_0'-T_\infty')}{\upsilon^2},\ Pr=\frac{\upsilon}{\alpha}, \\ &M=\frac{\sigma H_0^2 r_0^2}{\rho\nu}, P=\frac{k_f}{k_s}\ln\left(\frac{r_0}{r_i}\right) \end{aligned} \tag{10}$$

(the symbols are explained in the nomenclature) in the Eqs. (1)-(3), they reduced to the following form:

$$\frac{\partial U}{\partial X}+\frac{\partial V}{\partial R}+\frac{V}{R}=0 \tag{11}$$

$$\frac{\partial U}{\partial t}+U\frac{\partial U}{\partial X}+V\frac{\partial U}{\partial R}=T+\left(\frac{\partial^2 U}{\partial R^2}+\frac{1}{R}\frac{\partial U}{\partial R}\right)-MU \tag{12}$$

$$\frac{\partial T}{\partial t}+U\frac{\partial T}{\partial X}+V\frac{\partial T}{\partial R}=\frac{1}{\Pr}\left(\frac{\partial^2 T}{\partial R^2}+\frac{1}{R}\frac{\partial T}{\partial R}\right) \tag{13}$$

The corresponding initial and boundary conditions in non-dimensional quantities are given by

$$\begin{aligned} &t\le 0: U=0,\ V=0,\ T=0 \ \text{ for all } X \text{ and } R \\ &t>0: U=0,\ V=0,\ T-1=P\frac{\partial T}{\partial R} \ \text{ at } R=1 \\ &\qquad U=0,\ V=0,\ T=0 \ \text{ at } X=0 \\ &\qquad U\to 0,\ V\to 0, T\to 0 \ \text{ as } R\to\infty \end{aligned} \tag{14}$$

3. Numerical Procedure

In order to solve the unsteady coupled non-linear governing Eqs. (11)-(13) an implicit finite difference scheme of Crank-Nicolson type has been employed. The finite difference equations corresponding to Eqs. (11) - (13) are as follows:

$$\begin{aligned} &\frac{U_{i,j}^{k+1}-U_{i-1,j}^{k+1}+U_{i,j}^{k}-U_{i-1,j}^{k}}{\Delta X}+ \\ &\frac{V_{i,j+1}^{k+1}-V_{i,j-1}^{k+1}+V_{i,j+1}^{k}-V_{i,j-1}^{k}}{2\,\Delta R}+\frac{V_{i,j}^{k+1}+V_{i,j}^{k}}{\left[1+(j-1)\Delta R\right]}=0 \end{aligned} \tag{15}$$

$$\begin{aligned} &\frac{U_{i,j}^{k+1}-U_{i,j}^{k}}{\Delta t}+\frac{U_{i,j}^{k}}{2\,\Delta X}(U_{i,j}^{k+1}-U_{i-1,j}^{k+1}+U_{i,j}^{k}-U_{i-1,j}^{k}) \\ &\quad+\frac{V_{i,j}^{k}}{4\,\Delta R}(U_{i,j+1}^{k+1}-U_{i,j-1}^{k+1}+U_{i,j+1}^{k}-U_{i,j-1}^{k}) \\ &=\frac{T_{i,j}^{k+1}+T_{i,j}^{k}}{2}+\left(\frac{U_{i,j+1}^{k+1}-U_{i,j-1}^{k+1}+U_{i,j+1}^{k}-U_{i,j-1}^{k}}{4\left[1+(j-1)\Delta R\right]\Delta R}\right) \\ &\quad+\left(\frac{U_{i,j-1}^{k+1}-2U_{i,j}^{k+1}+U_{i,j+1}^{k+1}+U_{i,j-1}^{k}-2U_{i,j}^{k}+U_{i,j+1}^{k}}{2(\Delta R)^2}\right) \\ &\quad-M\left(\frac{U_{i,j}^{k+1}+U_{i,j}^{k}}{2}\right) \end{aligned} \tag{16}$$

$$\begin{aligned} &\frac{T_{i,j}^{k+1}-T_{i,j}^{k}}{\Delta t}+\frac{U_{i,j}^{k}}{2\Delta X}(T_{i,j}^{k+1}-T_{i-1,j}^{k+1}+T_{i,j}^{k}-T_{i-1,j}^{k}) \\ &\quad+\frac{V_{i,j}^{k}}{4\Delta R}(T_{i,j+1}^{k+1}-T_{i,j-1}^{k+1}+T_{i,j+1}^{k}-T_{i,j-1}^{k}) \\ &=\left(\frac{T_{i,j-1}^{k+1}-2T_{i,j}^{k+1}+T_{i,j+1}^{k+1}+T_{i,j-1}^{k}-2T_{i,j}^{k}+T_{i,j+1}^{k}}{2\Pr(\Delta R)^2}\right) \\ &\quad+\left(\frac{T_{i,j+1}^{k+1}-T_{i,j-1}^{k+1}+T_{i,j+1}^{k}-T_{i,j-1}^{k}}{4\Pr\left[1+(j-1)\Delta R\right]\Delta R}\right) \end{aligned} \tag{17}$$

To solve the finite difference Eqs. (15)-(17), the region of integration is considered as a rectangle composed of the lines indicating *Xmin* = 0, *Xmax* = 1, *Rmin* = 1 and *Rmax* = 16, where *Rmax* corresponds to $R = \infty$ which lies very far from the momentum and energy boundary layers. In the above Eqs. (15)-(17) the subscripts *i* and *j* designate the grid points along the *X* and *R* coordinates, respectively, where $X = i\,\Delta X$ and $R = 1 + (j-1)\,\Delta R$ and the superscript *k* designates a value of the time *t* (= $k\,\Delta t$), with ΔX, ΔR and Δt the mesh size in the *X*, *R* and t axes, respectively. In order to obtain an economical and reliable grid system for the computations, a grid independent test has been performed. The steady-state velocity and temperature values obtained with the grid system of 100 × 500 differ in the second decimal place from those with the grid system of 50 × 250, and in the fifth decimal place from those with the grid system of 200 × 1000. Hence, the grid system of 100 × 500 has been selected for all subsequent analyses, with mesh size in *X* and *R* direction are taken as 0.01 and 0.03, respectively. Also, the time step size dependency has been carried out, from which 0.01 yielded a reliable result.

From the initial conditions given in Eq. (14), the values of

velocity U, V and temperature T are known at time $t = 0$, then the values of T, U and V at the next time step can be calculated. Generally, when the above variables are known at $t = k\,\Delta t$, the variables at $t = (k + 1)\,\Delta t$ are calculated as follows. The finite difference Eqs. (16) and (17) at every internal nodal point on a particular i-level constitute a tridiagonal system of equations. Such a system of equations is solved by the Thomas algorithm [18]. At first, the temperature T is calculated from Eq. (17) at every j nodal point on a particular i-level at the $(k + 1)$th time step. By making use of these known values of T, the velocity U at the $(k+1)$th time step is calculated from Eq. (16) in a similar manner. Thus, the values of T and U are known at a particular i-level. Then the velocity V is calculated from Eq. (15) explicitly. This process is repeated for the consecutive i-levels; thus the values of T, U and V are known at all grid points in the rectangular region at the $(k + 1)$th time step. This iterative procedure is repeated for many time steps until the steady-state solution is reached. The steady-state solution is assumed to have been reached when the absolute difference between the values of velocity as well as temperature at two consecutive time steps is less than 10^{-5} at all grid points. The truncation error in the employed finite difference approximation is $O(\Delta t^2 + \Delta R^2 + \Delta X)$ and tends to zero as $\Delta X, \Delta R$ and $\Delta t \to 0$. Hence the system is compatible. Also, this finite difference scheme is unconditionally stable and therefore, stability and compatibility ensure convergence.

4. Results and Discussion

For the validation purpose, the present simulated velocity and temperature profiles are compared with those of the available steady-state, isothermal results of Lee et al.[4] for air ($Pr = 0.7$) without conduction and magnetic effects i.e., $P = 0.0$ and $M = 0.0$, as there are no experimental or analytical studies available to compare with the present problem. The current results are found to be in good agreement with the previous results available in literature as shown in Fig. 2.

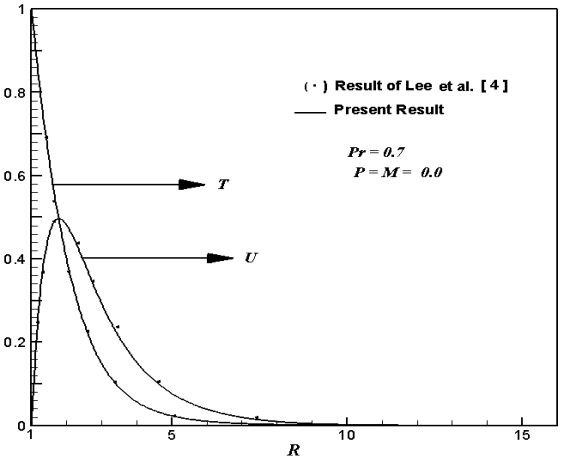

Figure 2. Comparison of the velocity and temperature profiles

The simulated results are presented to outline the general physics involved in the effects of different M (= 0.2, 0.5, 0.8 and 1.0) and P (= 0.1, 0.5, 1.0 and 2.0) with fixed Pr [= 0.71 (air)] on the transient velocity and temperature profiles. The simulated transient behaviour of the dimensionless flow variables, average wall shear stress and heat transfer rate are discussed in detail in the succeeding subsections.

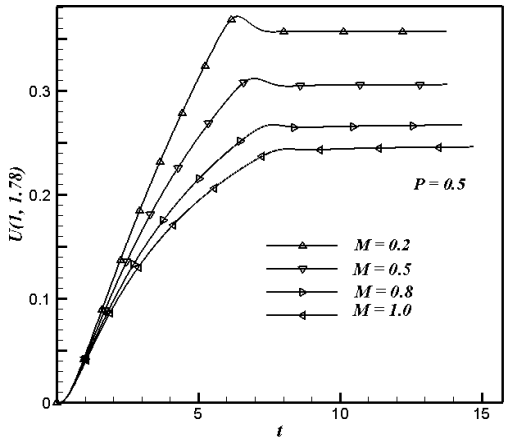

(3a)

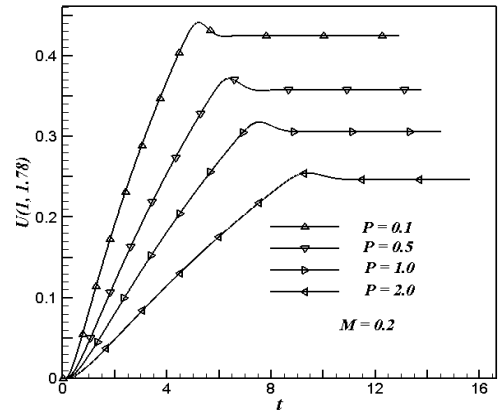

(3b)

Figure 3. The simulated transient velocity at (1, 1.78) for (a) variation of M ; (b) variation of P

4.1. Velocity

The simulated transient velocity (U) at (1, 1.78) for different values of magnetic parameter M and conjugate heat transfer parameter P against t is shown graphically in Fig. 3. Fig. 3a depicts the variation of M with fixed $P = 0.5$ and Fig. 3b for the variation of P with fixed $M = 0.2$. From Figs. 3a and 3b it is observed that the velocity increases with time, reaches a temporal maxima, then decreases and at last reaches the asymptotic steady-state. For example, in Fig. 3a when $M = 0.2$, the velocity increases with time monotonically from zero and reaches the temporal maximum, then slightly decreases with time and becomes asymptotically steady. It is observed that at the very early time (i.e., $t << 1$), the heat transfer is dominated by conduction. Shortly later, there exists a period when the heat transfer rate is influenced by the effect of convection with the increasing upward velocities along the time. When this transient period is almost

ending and just before the steady-state is about to be reached, there exist overshoots of the velocities. From Figs. 4a and 4b it can be observed that velocity profiles reach their maximum value approximately at (1, 1.78). Similarly, the velocity at other locations also exhibits somewhat similar transient behaviour. As noted in Fig. 3a, the magnitude of this overshoot of the velocities decreases as M is increased, since with the increasing M the velocity diffusion is increased (refer Eq. (12)). Hence, there is a high resistance to the fluid flow in the region of the temporal maximum of velocity. The time needed to reach the temporal maximum of the velocity increases as M increases. It is also noticed that for small values of M the temporal maximum is reached at early times. For all values of P, Figure 3b reveals that it has the same trend as the transient behaviour with respect to M shown in Fig. 3a, but the temporal maximum of velocity decreases as P increases. In association with the transient characteristics of the velocity, similar trends of the temperature fluctuation can be observed and will be described in Fig. 5.

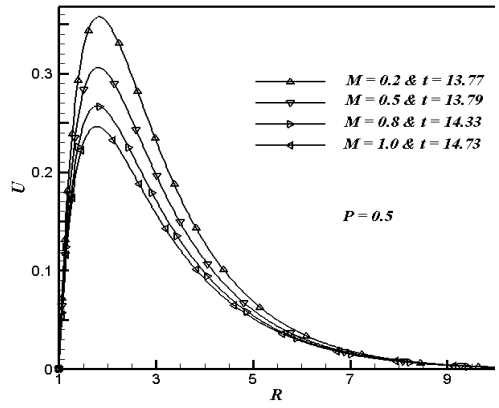

(4a)

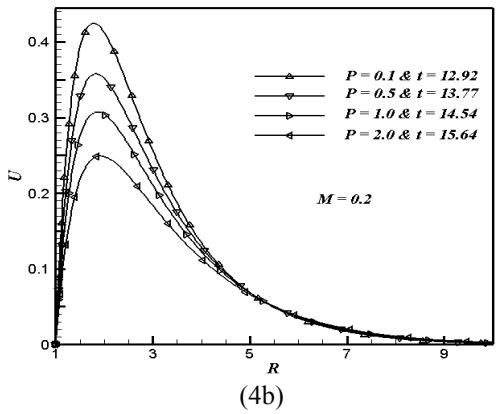

(4b)

Figure 4. The simulated steady-state velocity profile at X =1.0 for (a) variation of M ; (b) variation of P

Figure 4 depicts the simulated steady-state velocity profiles against the R at X = 1.0 for different values of M and P. Fig. 4a shows the variation of M with fixed P = 0.5 and Fig. 4b for the variation of P with fixed M = 0.2. From these figures it is observed that the velocity profile start with the value zero at the wall, reach their maximum and then monotonically decrease to zero along the radial coordinate for all t. Also it is observed that in the vicinity of the wall the magnitude of the axial velocity is rapidly increasing as R increases from R_{min} (=1). From Fig. 4a it is observed that the velocity decreases with the increasing values of M because the effect of velocity diffusion gets increased for high values of M. The magnetic parameter M , representing the Lorentz force, which opposes the flow. The peak velocity decreases with the in creasing M due to this retarding effect as shown in Fig. 4a. As a result, the separation of the boundary layer occurs earlier since the momentum boundary layer becomes thicker. When M is increased, the thermal convection is confined to a region near the hot wall, while the momentum diffusion is propagated far from the hot wall and hence the high velocity profiles are observed close to the hot wall. It is also observed that the time required to reach the steady-state increases as M increases. Fig. 4b reveals that it has the same trend as the variation of steady-state time with respect to M as shown in Fig. 4a, but the velocity profile is influenced significantly and decreases when the value of P increases.

4.2. Temperature

The simulated transient temperature (T) for different values of M and P with respect to t is shown at the point (1, 1.15)

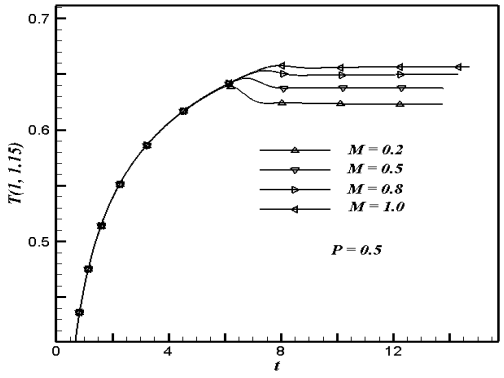

(5a)

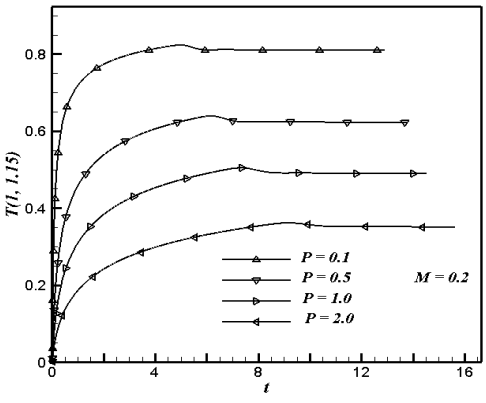

(5b)

Figure 5. The simulated transient temperature at (1, 1.15) for (a) variation of M ; (b) variation of P

in Fig. 5. Figure 5a shows the variation of M with fixed P = 0.5 and Fig. 5b for the variation of P with fixed M = 0.2. From Figs. 5a and 5b it is observed that these profiles increase with time, reach a temporal maxima, decrease and again after a slight increase attain the steady-state asymp-

totically. The temperature at other locations also exhibits somewhat similar transient behaviour. During the initial period, the nature of the transient temperature profiles is particularly noticeable. From Fig. 5a it is observed that for all values of M, the transient temperature profiles initially coincide and then deviate after some time. Also, the time required to reach the temporal maximum of the temperature increases with the increasing values of M. It can be noticed that for small values of M the temporal maximum is attained at an early times. Here, it is observed that the maximum value of temperature increases with the increasing M. Figure 6b shows that it has the same trend as the transient behaviour with respect to M shown in Fig. 5a, but the temporal maximum of temperature decreases as P increases. From Figs. 5a and 5b it is noticed that during the initial time, the variation of temperature with P is observed to be larger than that with M. This result implies that the temperature field is more strongly affected by the conjugate heat transfer parameter, since an increased value of P corresponds to a lower wall conductance k_s and promotes larger surface temperature variations as mentioned in Fig. 5b.

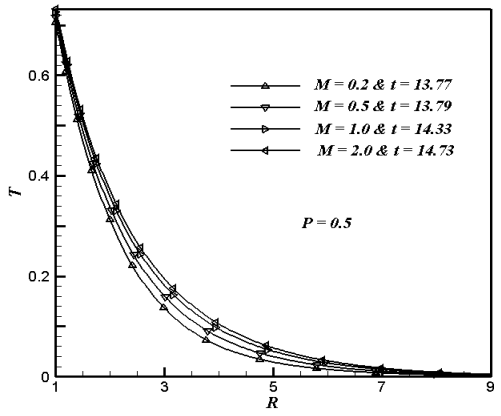

(6a)

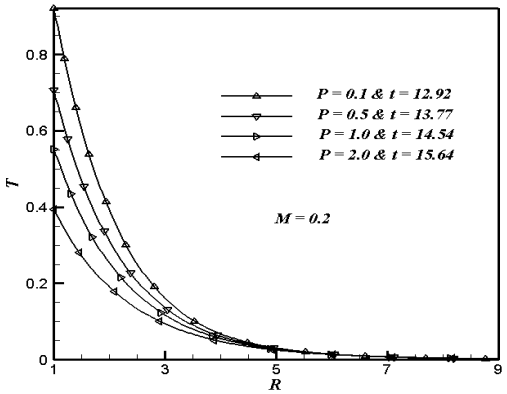

(6b)

Figure 6. The simulated steady-state temperature profile at $X = 1.0$ for (a) variation of M ; (b) variation of P

The simulated steady-state temperature profiles for different values of M and P at $X = 1.0$ against the R are shown in Fig. 6. Figure 6a reveals the variation of M with fixed $P = 0.5$ and Fig. 6b for the variation of P with fixed $M = 0.2$. From these figures it is observed that the temperature profiles start with the hot wall temperature and then monotonically decrease to zero along the radial coordinate for all time. It is related to the fact that the effect of velocity diffusion gets increased for higher values of P, which allows higher velocity near the hot wall. From Fig. 6a it is observed that the steady temperature value increases with increasing values of M for fixed P. Larger M values give rise to thicker temperature profiles, since a larger M value means that the thermal diffusion from the wall is prevailing while the velocity diffusion tries to move close to the wall. The increased value of the magnetic parameter increases the thickness of the thermal boundary layer . Temperature at the interface also varies since the conduction is considered with in the cylinder. Also, time taken to reach the steady-state increases as M increases. Figure 6b reveals that the steady temperature value decreases as the heat transfer parameter P increases. A lower wall conductance k_s or greater convective cooling effect due to larger k_f increases the value of P as well as causes higher temperature difference between the two surfaces of the cylinder. This is due to the reason that the temperature at the solid-fluid interface is decreased since the temperature at the inner surface of the cylinder is kept constant. As a result the temperature profile as well as the velocity profile moves downwards in the fluid. It is also observed that the time taken to reach the steady-state increases with increasing values of P.

4.3. Average Skin-friction Coefficient and Heat Transfer Rate

For engineering purposes, one is usually interested in the values of the skin-friction coefficient and heat transfer rate. The friction coefficient is an important parameter in the heat transfer studies since it is directly related to the heat transfer coefficient. The increased skin-friction is generally a disadvantage in technical applications, while the increased heat transfer can be exploited in some applications such as heat exchangers, but should be avoided in others such as gas turbine applications, for instance. For the present problem these skin-friction coefficient and heat transfer rate are derived and given in the following equations:

The wall shear stress at the wall can be expressed as

$$\tau_w = \left(\mu \frac{\partial u}{\partial r}\right)_{r=r_0} \tag{18}$$

By introducing the non-dimensional quantities given in Eq. (10), the above Eq. (18) can be written as

$$\tau_w = \frac{\mu^2 Gr}{\rho r_0^2}\left(\frac{\partial U}{\partial R}\right)_{R=1} \tag{19}$$

Considering $\frac{\mu^2 Gr}{\rho r_0^2}$ to be the characteristic shear stress, then the local skin-friction coefficient can be written as

$$C_f = \left(\frac{\partial U}{\partial R}\right)_{R=1} \tag{20}$$

The integration of the Eq. (20) from $X = 0$ to $X = 1$ gives the following average skin-friction coefficient.

$$\overline{C_f} = \int_0^1 \left(\frac{\partial U}{\partial R}\right)_{R=1} dX \tag{21}$$

The local Nusselt number is given by

$$Nu_x = \frac{\dot{q}_w r_0}{k_f (T_0' - T_\infty')} \tag{22}$$

where the heat transfer, $\dot{q}_w$ is given by

$$\dot{q}_w = -k_f \left(\frac{\partial T'}{\partial r} \right)_{r=r_0}$$

Thus, with the non-dimensional quantities introduced in Eq. (10), Eq. (22) can be written as

$$Nu_X = -\left(\frac{\partial T}{\partial R} \right)_{R=1} \tag{23}$$

The integration of the above Eq. (23) with respect to X from 0 to 1 yields the following average Nusselt number.

$$\overline{Nu} = -\int_0^1 \left(\frac{\partial T}{\partial R} \right)_{R=1} dX \tag{24}$$

The derivatives involved in Eqs. (21) and (24) are evaluated by using a five-point approximation formula and then the integrals are evaluated by using the Newton-Cotes closed integration formula. The simulated average non-dimensional skin-friction and heat transfer coefficients have been plotted against the time in Figs. 7 and 8 for different values of M and P.

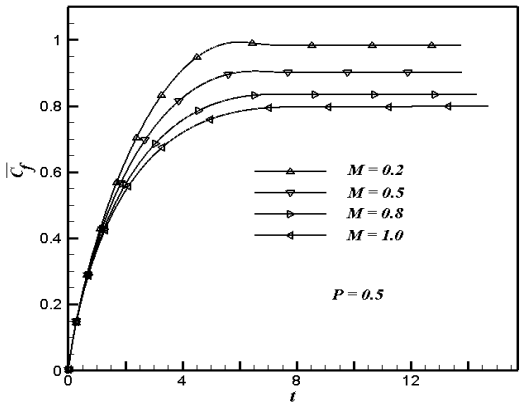

(7a)

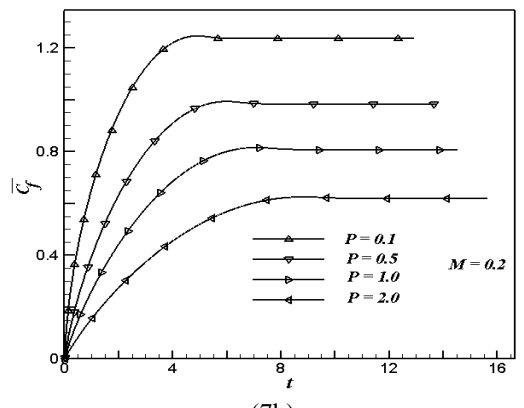

(7b)

Figure 7. The simulated average skin-friction for (a) variation of M ; (b) variation of P

The effects of different values of M and P on the simulated average skin-friction coefficient are shown in Figs. 7a and 7b, respectively. From Figs. 7a and 7b it is observed that for all values of M and P the average skin-friction coefficient increases with time, attains the maximum value and, after slight decrease, reaches asymptotically steady-state. Because the buoyancy-induced flow velocity is relatively low at the initial transient period, as seen in Fig. 3, the wall shear stress remain small, as shown in Fig. 7. However, the wall shear stress increases as the time proceeds, yielding an increase in the skin-friction coefficient. It is also observed from Fig. 7a that for increasing values of M the average skin-friction coefficient decreases. This result lies in the same line with the velocity profiles plotted in Fig 4a. The magnetic force opposes the flow , as mentioned previously, and reduces the wall shear stress. From Fig. 7b it is observed that the average skin-friction coefficient decreases as P increases. It is related to the fact that the increased value of P decreases the velocity of the fluid within the boundary layer region, as mentioned in Fig. 4b, and decreases the viscosity of the fluid. It is also noticed that from Figs. 7a and 7b during the initial period, the variation of skin-friction with P is observed to be larger than that with M. This result means that the average skin-friction coefficient is more strongly affected by P compared to the magnetic parameter M.

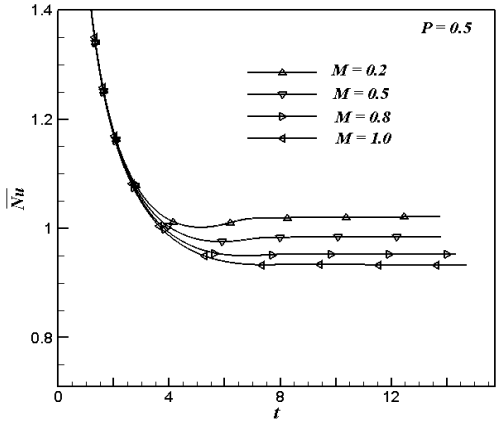

(8a)

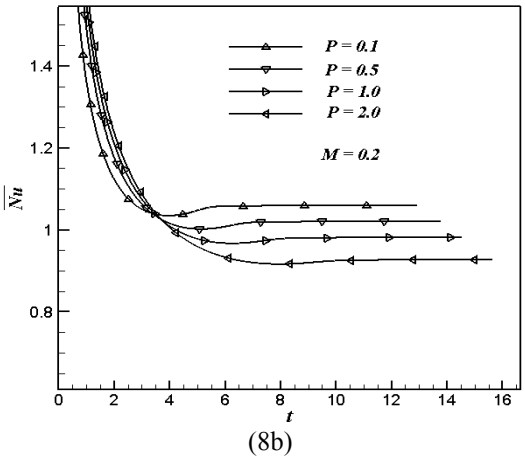

(8b)

Figure 8. The simulated average Nusselt number for (a) variation of M ; (b) variation of P

In Figs. 8a and 8b the effects of different values of M and P on the simulated average heat transfer rate are shown, respectively. From Figs. 8a and 8b it is observed that at short times, after $t = 0$, the average Nusselt numbers are almost the

same for all values of P and M. This shows that initially there is only heat conduction. Fig. 8a reveals that an increase in the value of M leads to a decrease in the values of the average heat transfer rate. Increasing M retards the spatial decay of the temperature field near the heated surface because of increased flow velocity near the wall, yielding a decrease in the rate of heat transfer. Further the heat transfer rate depends on the gradient of temperature. As the gradient decreases with the increasing M, the average heat transfer rate also decreases. From Fig. 8b it is observed that with the increasing values of P i.e with lower wall conductance (k_s), the average heat transfer rate decreases as P increases.

5. Conclusions

Conjugate heat transfer analysis on unsteady natural convection hydromagnetic flow of a viscous incompressible fluid over a vertical slender hollow cylinder has been studied. An implicit finite difference scheme of Crank-Nicolson type has been used to solve the governing unsteady, non-linear and coupled equations. The resulting system of equations is solved by using the tridiagonal algorithm. The computations are carried out for different values of magnetic parameter M (= 0.2, 0.5, 0.8 and 1.0) and conjugate heat transfer parameter P (= 0.1, 0.5, 1.0 and 2.0). For the velocity and temperature profiles it is observed that the time elapsed to reach the temporal maximum increases with the increasing values of M and P. Time needed to reach the steady-state increases as M and P increases. It is noticed that the velocity and average skin-friction coefficient of the fluid decreases with the increasing values of M. The values of flow variables (U, T) of the fluid decreases as P increases. It is also observed that as P or M increases the steady-state values of average Nusselt number decreases.

Nomenclature

$\overline{c_f}$	dimensionless average skin-friction coefficient
c_f	dimensionless local skin-friction coefficient
c_p	specific heat at constant pressure
g	acceleration due to gravity
Gr	Grashof number
H_0	applied magnetic field
k_f, k_s	thermal conductivity of the fluid and the solid cylinder, respectively
l	length of the cylinder
M	magnetic parameter
$\overline{Nu}$	dimensionless average Nusselt number
Nu_X	dimensionless local Nusselt number
P	conjugate heat transfer parameter
Pr	Prandtl number
r	radial coordinate
r_i, r_0	inner and outer radii of the hollow cylinder, respectively
R	dimensionless radial coordinate
t'	time
t	dimensionless time
T_0'	temperature at the inside surface of the cylinder
T_s'	solid temperature
T'	temperature of the fluid
T	dimensionless temperature of the fluid
u, v	velocity components in x, r directions respectively
U, V	dimensionless velocity components in X, R directions respectively
x	axial coordinate
X	dimensionless axial coordinate

Greek Letters

α	thermal diffusivity
β	volumetric coefficient of thermal expansion
ρ	density
σ	electrical conductivity of the fluid
μ	viscosity of the fluid
υ	kinematic viscosity

Subscripts

w	conditions on the wall
∞	free stream conditions

ACKNOWLEDGEMENTS

The authors wished to acknowledge support for this research work from the Institute Fellowship (National Institute of Technology Warangal).

REFERENCES

[1] Sparrow, E. M., and Gregg, J. L., 1956, Laminar free convection heat transfer from the outer surface of a vertical circular cylinder, ASME Journal of Heat Transfer, 78, 1823-1829.

[2] Velusamy, K., and Garg, V.K., 1992, Transient natural convection over a heat generating vertical cylinder. Interna tional Journal of Heat and Mass Transfer, 35, 1293–1306.

[3] Fujii, T., and Uehara, H., 1970, Laminar natural convective heat transfer from the outer surface of a vertical cylinder, International Journal of Heat and Mass Transfer, 13, 607-615.

[4] Lee, H. R., Chen, T. S., and Armaly, B. F., 1988, Natural convection along slender vertical cylinders with variable surface temperature, ASME Journal of Heat Transfer, 110, 103-108.

[5] Ganesan, P., and Rani, H. P., 1998, Transient natural convec tion along vertical cylinder with heat and mass transfer, Heat Mass Transfer, 33, 449–454.

[6] Rani, H. P., and Kim, C. N., 2008, Transient free convection flow over an isothermal vertical cylinder with temperature dependent viscosity, Korean Journal of Chemical Engineering, 25, 34-40.

[7] Mendez, F., Trevino, C., 2000, The conjugate conduction-natural convection heat transfer along a thin vertical

plate with non-uniform internal heat generation, International Journal of Heat and Mass Transfer, 43, 2739–2748.

[8] Bautista, O., Mendez, F., and Trevino, C., 2000, Graetz problem for the conjugated-conduction film condensation process, Journal of Thermophysics and Heat Transfer, 14, 1–7.

[9] Trevino, C., Espinoza, A., and Mendez, F., 1996, Steady state analysis of the conjugate heat transfer between forced counter flowing streams, Journal of Thermophysics and Heat Transfer, 10, 476–483.

[10] Gdalevich, L. B., and Fertman, V. E., 1977, Conjugate Problems of Natural Convection, Inzh-Fiz. Zh., 33, 539-547.

[11] Miyamoto, M., Sumikawa, J., Akiyoshi, T., and Nakamura, T., 1980, Effects of Axial Heat Conduction in a Vertical Flat Plate on Free Convection Heat Transfer, International Journal of Heat and Mass Transfer, 23, 1545-1553.

[12] Pozzi, A., and Lupo, M., 1988, The coupling of conduction with laminar natural convection along a flat plate, International Journal of Heat and Mass Transfer, 31, 1807–1814.

[13] Vynnycky, M., and Kimura, S., Transient conjugate free con vection due to a heated vertical plate, International Journal of Heat and Mass Transfer, 39, pp. 1067–1080, 1996

[14] Ahmet Kaya, 2011, Effects of buoyancy and conjugate heat transfer on non-Darcy mixed convection about a vertical slender hollow cylinder embedded in a porous medium with high porosity, International Journal of Heat and Mass Transfer, 54, 818-825.

[15] Chamkha, A. J., and Camille, I., 2000, Effects of heat generation/absorption and the thermophoresis on hydromagnetic flow with heat and mass transfer over a flat plate, International Journal of Numerical Methods and Heat Fluid Flow, 10, 432–448.

[16] Mamun, A. A., Chowdhury, Z. R., Azim, M. A., and Molla, M. M., 2008, MHD-conjugate heat transfer analysis for a vertical flat plate in presence of viscous dissipation and heat generation, International Communications in Heat and Mass Transfer, 35, 1275-1280.

[17] Chang, C. L., 2006, Buoyancy and wall conduction effects on forced convection of micropolar fluid flow along a vertical slender hollow circular cylinder, International Journal of Heat and Mass Transfer, 49, 4932-4942.

[18] B. Carnahan, H. A. Luther and J. O. Wilkes, Applied numerical methods, John Wiley Sons, New York, 1969.